The Role of Polymerizable Organophilic Clay During Preparing Polyethylene Nanocomposite via Filling Polymerization

Changyi Ren,[1,2] Xiaohua Du,[1,2] Li Ma,[1] Yanhui Wang,[1] Tao Tang[1]

[1]*State Key Laboratory of Polymer Physics and Chemistry, Changchun Institute of Applied Chemistry, Chinese Academy of Sciences, Changchun 130022, China*
[2]*Graduate School of the Chinese Academy of Sciences, Beijing 100039, China*

Received 22 October 2009; accepted 29 December 2009
DOI 10.1002/app.32040
Published online 29 March 2010 in Wiley InterScience (www.interscience.wiley.com).

ABSTRACT: Effect of polymerizable montmorillonites (P-MMTs) on the morphology of polyethylene/montmorillonites (PE/MMTs) nanocomposites during filling polymerization was studied. The microstructure analysis showed that the P-MMTs were more exfoliatable than nonpolymerizable MMTs in the preparation of PE/MMTs nanocomposites. By examining the influence of the polymerization condition on the microstructure of the resultant nanocomposites, it was confirmed that the shear force formed by the mechanical stirring was the driving force of the exfoliation dispersion of MMT sheets during the filling polymerization. Comparatively, the shear force on MMT sheets might be increased due to strong interaction between PE chains linked to the surface of P-MMTs and the solvents molecules, which is the reason that polymerizable clay is more exfoliatable than nonpolymerizable clay. The copolymerization between polymerizable modifier and ethylene was confirmed by NMR measurements. Furthermore, the morphology of the resultant nanocomposites was influenced by the concentration of the dispersed P-MMTs. The degree of exfoliation of the resultant nanocomposites at a relatively low concentration was higher than that at a high concentration. This is because of the multiscale organization of the organoclay dispersed in the organic medium. High exfoliation degree of MMTs and improved interaction between PE matrix and P-MMTs in PE/P-MMTs nanocomposites led to significant improvements in mechanical properties and barrier properties. © 2010 Wiley Periodicals, Inc. J Appl Polym Sci 117: 1646–1657, 2010

Key words: clay; nanocomposites; polyethylene (PE); polymerization

INTRODUCTION

As the discovery of remarkable improvements in physical properties of polymeric materials with addition of small amounts of clay,[1–3] researchers have placed heavy emphasis on the synthesis of polymer/clay nanocomposites.[4–6] Such enhancements in properties have been attributed to the nanoscale dimensions of clay particles, which allow significant polymer–clay interaction. The most significant enhancements have been observed with complete delamination of the clay platelet (exfoliation). The clay particles may also be dispersed in aggregates that retain their ordered morphology (intercalated state) with polymer embedded between clay sheets. The most frequently observed morphology is a mixture of intercalated and exfoliated domains. To aid the dispersion and the exfoliation of clay in organic media, hydrophilic clay particles are typically modified with quaternary ammonium surfactants. Even with the incorporation of quaternary ammonium surfactants, complete exfoliation of clay particles is usually difficult. Different mechanical and chemical means have been utilized to facilitate exfoliation to varying degrees of success. Three principal strategies have been investigated to obtain polymer/clay nanocomposites, including solution-blending,[7,8] melt intercalation[9–12] and *in situ* polymerization.[13,14]

Besides *in situ* intercalative polymerization, in which the polymerization is initiated in the gallery of organoclay (or clay) to exfoliate the clay aggregate when the polymer chains grow in size, polymer/clay nanocomposites can also be obtained by filling polymerization. In this process, the organoclay (or clay) is added into the reaction system, where it may be intercalated or even exfoliated by solvent or monomer molecules (for bulk polymerization, monomers serving as solvents) during the polymerization, and the nanocomposite is *in situ* formed. In this case, the dispersion state of the organoclay in the systems is vital to the final morphology of the resultant nanocomposite.[15,16] Generally organoclays are well known in their ability for swelling and gel formation in organic media.[15,17–20] The dispersion state

Correspondence to: T. Tang (ttang@ciac.jl.cn).
Contract grant sponsor: National Natural Science Foundation of China; contract grant numbers: 50525311, 20734006, 50921062.

© 2010 Wiley Periodicals, Inc.

of organoclay in the organic media depends on the interactions between the media and the surface of organoclay at different scales, i.e., swelling at the macroscopic scale to form gels, interplatelets swelling at nanoscopic scale.[15,19–21] Enhanced dispersions could be induced by increasing the interaction between the monomers and the organoclays.[16] If the organoclay is exfoliated in the solvent or monomer, then exfoliated nanocomposite would be obtained; if the organoclay is intercalated in the organic medium, then the morphology of the resultant nanocomposite usually is an intercalated structure.

Efforts had been made to promote the exfoliation of the clay platelets in the filling polymerization. It has been found that the introduction of polymerizable groups into the clay galleries can lead to a more exfoliated morphology of the organoclay. This method has been mostly reported in the preparation of polystyrene (PS)/clay nanocomposites.[22–30] It can also be used in the preparation of other polymer/clay nanocomposites.[16,31–36] According to these researches, the resultant nanocomposite is usually intercalated whether the modified clay by nonpolymerizable agent is intercalated or not in the system before polymerization; but the resultant nanocomposite is usually partially exfoliated when the modified clay by polymerizable agent is intercalated in the system before polymerization. If the modified clay is exfoliated in the system before polymerization, no matter the clay is polymerizable or not, the resultant nanocomposite is surely exfoliated. Furthermore, the use of polymerizable clay can also bring enhanced interfacial interaction between polymer matrix and clay through the copolymerization of polymerizable modifiers and monomers, which would bring enhanced properties consequently, e.g. improved thermal stability, mechanical properties, and increased glass transition temperature. Furthermore, some researchers suggested that the exfoliation degree of the polymerizable clay could be influenced by the position of the reactive functional group,[16,24,37] and a crosslinking structure was found during the preparation.[25,28,32,33,37] However, the reason why the polymerizable clay is more exfoliatable than the nonpolymerizable clay is still unclear. Obviously, such knowledge could be very useful in designing exfoliated nanocomposites with enhanced interfacial interaction.

Polyolefin is a kind of the most widely used polymers for many applications due to their low cost and high performance, thus the polyolefin/clay nanocomposites are highly attractive.[38–40] But polyolefin does not have polar groups in its backbone and is not compatible with clays. So the filling polymerization involving polymerizable clay is the desirable solution to the preparation of polyolefin/clay nanocomposites.[40–45] In this work, we use the filling polymerization to prepare polyethylene (PE)/MMTs nanocomposites through polymerizing ethylene catalyzed by metallocene/MAO system in the presence of polymerizable MMTs (P-MMTs). We focus on investigating microstructure evolution in the resultant nanocomposites and the driving force of exfoliated dispersion of P-MMTs. The effects of polymerization conditions, such as the concentration of P-MMTs, stirring rate, and polymerization time, on the microstructures of the resultant nanocomposites were studied. The shear force formed by mechanical stirring, of which the transmission could be influenced by the interaction between the polymer chains linked to clay and the solvent molecules, plays a key role in the formation of the final microstructure of the nanocomposites.

EXPERIMENTAL

Materials

Na^+-montmorillonites (MMTs) used in this work, with a cation exchange capacity (CEC) of 119 mequiv/100g, were from Kunimine Co. Analytical grade Na_2SO_4, KOH, C_2H_5OH, and dodecylamine were used without further purification. *N*,*N*-dimethyllformamide (DMF) was dried over 4 Å molecular sieves for 10 days and then distilled over CaH_2 under vacuum. Toluene was dried over 4 Å molecular sieves for 10 days and then refluxed over Na/K alloy for at least 8 h and distilled. 11-Bromo-undecene (95%, Aldrich), phthalimide (98%, Aldrich), *rac*-ethylene bis(4,5,6,7-tetra-hydro-1-indenyl) zirconium dichloride (*rac*-Et$(IndH_4)_2ZrCl_2$, Boulder Scientific Company), methylaluminoxane (MAO: 10 wt % in toluene, Ethyl Corp.), and ethylene (polymerization grade, Liaoyang Chemical Corp.) were used without further treatment.

Preparation of samples

Undec-10-enylamine, which was used as a precursor of modifier for the MMTs, was synthesized through Gabriel method according to the reference method.[46] Then the precursor was protonated with equal molar concentrated HCl in deionized water at 80°C to get undec-10-enylammonium chloride as a modifier. Polymerizable montmorillonites (P-MMTs) were prepared by ion exchange of undec-10-enylammonium chloride with interlamellar cations of the MMTs. The hot aqueous solution of modifier was poured into the hot dispersion of MMTs, and the loading level of the modifier was 143 mequiv/100g, which is 1.2 CEC times. The mixture was stirred vigorously for 30 min at 80°C, then filtrated, washed with 50% (v/v) aqueous ethanol and freeze-dried for 24 h. Synthesis of polyethylene/P-MMTs (PE/P-MMTs)

nanocomposites was performed at 60°C with 1.2 bar of ethylene pressure in a glass reactor with toluene as the solvent. Before polymerization, the glass reactor was heated under vacuum and allowed to cool down under dry argon flow to remove all moisture traces. After transferring 100 mL toluene and designed amount of P-MMTs to the reactor, the mixture was stirred at 60°C for 2 h to make the P-MMTs swollen sufficiently in the toluene. Then the prescribed amounts of MAO and catalyst (Al/Zr = 1500) were transferred to the reactor, and polymerization was started by pressurizing the reactor with ethylene under the mechanical stirring rate of 350 rpm. After 1 h, the polymerization was stopped by rapid depressurization of the reactor and quenching with ethanol. The reaction mixture was precipitated in ethanol above 5 h and then filtered, washed with ethanol, and dried in a vacuum oven overnight. Samples were marked as P-PEx (x = 1 to 5) according to their contents of P-MMTs. PE/dodecylammonium chloride modified MMTs (PE/12MMTs) composites were synthesized to compare with PE/P-MMTs nanocomposite. On the basis of theoretical models,[47,48] increasing the length of organic molecules tethered on clays is a promising approach to further promote the dispersion of clay sheets in a polymer matrix, surely PE/12MMTs composite should have better performance in the dispersion state of clay sheets than PE/undecylammonium (not available) modified MMTs composite. All experimental conditions were kept the same. Samples with different content of 12MMTs were marked as 12PEx (x = 1 to 3). A neat PE sample was also prepared for comparison, marked as HOMO.

Characterization

Wide angle X-ray diffraction (WAXD) was carried out with a Rigaku model Dmax 2500 using a Cu Kα radiation, and the interlayer distance (d_{001}) of MMTs was estimated from the (001) diffraction peak in the WAXD profiles with Bragg formula. All high-temperature ^{1}H-NMR and ^{13}C-NMR spectra were recorded on a Bruker AM-400 instrument in *o*-dichlorobenzene (DCB) -d_4 at 130°C. Molecular weight and molecular weight distribution of the products were measured with gel permeation chromatography (GPC) operated at 135°C and equipped with four Waters Styragel columns (HMW2, 2×HMW6W, HMW7) and a RI detector. 1,2,4-trichlorobenzene was applied as solvent at a flow rate of 1.0 cm^3/min. The columns were calibrated with narrow molar mass distribution polystyrene standards using a universal calibration method. Before examination the samples were dissolved in 1,2,4-trichlorobenzene and then filtrated. For all the samples with low MMT contents, only few MMT platelets would pass through the columns, and the effect of MMT sheets on GPC results could be neglected. Field emission scanning electron microscope (FESEM) and energy-dispersive X-ray (EDX) analysis were used to investigate the morphology and the composition of the samples on a XL 30 ESEM FEG scanning electron microscope (Micrio Fei Philips, Holand). Transmission electron microscope (TEM, JEOL JEM-2010(HR), at 200 kV) was also used to investigate the morphology of PE nanocomposites. Samples were prepared using ultramicrotome at −100°C. Thermal gravimetric analysis (TGA) was carried out on a PerkinElmer TGA-7 Series Thermal Analysis System at a heating rate of 10°C/min from 50 to 700°C under nitrogen gas. Rheological measurements were performed on a PHYSICA MCR 300 at 190°C, and complex viscosities and storage modulus were measured as a function of angular frequency (ranging from 0.01 to 100 rad/s). Static mechanical properties were measured with Instron 1121 tensile testing machine, and the crosshead rate was set at 20 mm/min. The data showed good repeatability. The permeation experiments of oxygen through neat PE film and the nanocomposite films were measured with a gas transmission rate (G.T.R.) measurement apparatus (K-315-N-03) at 30°C. The thickness of the samples was about 30 μm.

RESULTS AND DISCUSSION

Syntheses of polymerizable montmorillonites (P-MMTs) and PE/P-MMTs nanocomposites

Undec-10-enylamine was synthesized through Gabriel synthesis method[46] (45% yield), and the structure was confirmed by ^{1}H-NMR (Fig. 1). Polymerizable organic modifier was synthesized by protonating the undec-10-enylamine with equal molar concentrated HCl. P-MMTs were prepared by intercalation of the earlier modifier into the interlayer of MMTs via cation exchange. At the same time dodecylammonium chloride modified MMTs (12MMTs) were prepared for comparison. Figure 2 shows that a distinct shift of the (001) diffraction peak in the wide angle X-ray diffraction (WAXD) profiles of P-MMTs (2θ = 6.3°, d_{001} = 1.40 nm) and 12MMTs (2θ = 6.2°, d_{001} = 1.42 nm) occurs in

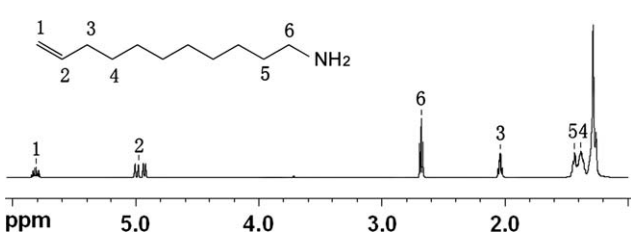

Figure 1 ^{1}H-NMR spectrum of Undec-10-enylamine in $CDCl_3$-d_1.

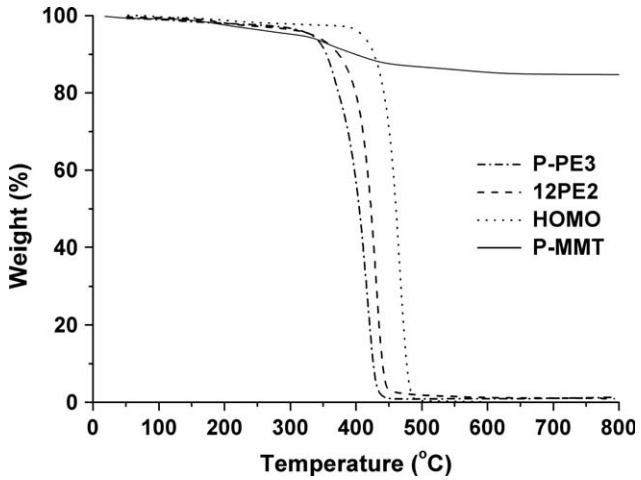

Figure 2 TGA results of P-MMT, HOMO, 12PE2 (12MMT 1.0 wt %), and P-PE3 (P-MMT 1.0 wt %).

contrast with that of MMTs ($2\theta = 8.9°$, $d_{001} = 9.92$ nm), which indicates an effective intercalation of the organic modifiers. TGA results of P-MMTs, HOMO, 12PE2, and P-PE3 were shown in Figure 2. It showed that P-MMTs contained about 14.1 wt % of the organic modifier (marked as wt $\%_{PM}$), which was 80.7% with respect to the CEC of MMTs (marked as $E\%_{PM}$). Comparatively, 12PE2 and P-PE3 showed a worse thermal stability than HOMO due to the introduction of quaternary ammonium modified MMT. Quaternary ammonium was typically poor thermostable.

Table I summarizes the results of ethylene polymerization catalyzed by *rac*-Et$(IndH_4)_2ZrCl_2$ in the presence of organically modified MMTs (OMMTs). Weight-average molecular weight (M_w) and polydispersity index (PDI), and the MMT contents of all the samples were measured by GPC and TGA, respectively. Before GPC measurements, the samples were dissolved in 1,2,4-trichlorobenzene then filtered through a filter with its aperture about 200 nm in diameter. Thus there would be almost no MMT sheets or PE molecules linked to the MMTs passing through the filter in the solution for GPC measurements. Based on the GPC results, the M_w of PE in PE/P-MMTs nanocomposites (P-PE1P-PE4) decreased in comparison with that of neat PE (HOMO sample in Table I). The same phenomenon was also reported in other researches where copolymerizable monomers took part in polymerization.[49,50] In contrast, the M_w of PE in PE/12MMTs composite (12PE1) is close to that of the neat PE. For P-PE5, homopolymerized PE and copolymerized PE were separated by extraction using decalin as solvent in a Soxhlet extractor for 48 h, and then the MMTs in the residue were removed by reacting with hydrogen fluoride (HF) before examination. According to the GPC results for the both parts, it is clear that the M_w of homopolymerized PE is higher than that of copolymerized PE. The catalytic activities decreased slightly in the presence of OMMTs. While comparing PE/P-MMTs nanocomposites with PE/12MMTs composites, the activity of the catalyst almost remained the same. Under the same polymerization conditions, the contents of MMTs in the PE/P-MMTs nanocomposites and the PE/12MMTs composites increased with the concentration of OMMTs.

TABLE I
Summary for the Filling Polymerization Results of Ethylene in the Presence of Fillers Using *rac*-Et$(IndH_4)_2ZrCl_2$ as Catalyst[a] and d_{001} Values of MMT in the Resultant PE/MMT Nanocomposites

Samples	MMTs content[b] (wt %)	MMT d_{001}[c] (nm)	Activity[d] (10^6g/atm h mol)	M_w[e] (10^5g/mol)	M_n[e] (10^4g/mol)	PDI
P-PE1[f]	0.2	null	2.24	1.33	4.75	2.8
P-PE2[f]	0.4	null	2.01	1.28	3.88	3.3
P-PE3[f]	1.0	1.40	1.98	1.26	5.04	2.5
P-PE4[f]	2.5	1.40	1.76	1.52	5.85	2.6
P-PE5[f]	3.7	1.40	1.90	1.14	6.33	1.8
P-PE5[f,g]	null	1.40	null	0.75	2.78	2.7
12PE1[h]	0.4	1.42	2.16	2.14	8.92	2.4
12PE2[h]	1.0	1.42	1.89	2.03	8.46	2.4
12PE3[h]	5.6	1.42	2.08	null	null	null
HOMO	null	null	2.20	2.27	8.41	2.7

[a] Polymerization conditions: temperature = 60°C, $P_{ethylene} = 1.2$ bar, [*rac*-Et$(IndH_4)_2ZrCl_2$] = 3.42×10^{-5} M, Al/Zr = 1500, time = 1 h, stirring rate = 350 rpm.
[b] Measured by TGA.
[c] Calculated according to WAXD results.
[d] Activity = resultant product mass/(time × [*rac*-Et$(IndH_4)_2ZrCl_2$] × $P_{ethylene}$).
[e] Measured by GPC.
[f] PE/P-MMT nanocomposite.
[g] The remains of P-PE5 after extracted by decalin and then HF treatment.
[h] PE/12MMT nanocomposite.

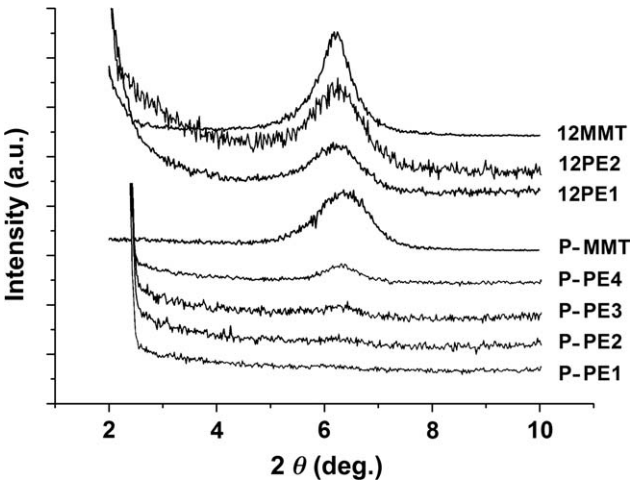

Figure 3 WAXD profiles of PE/12MMTs and PE/P-MMTs samples.

Morphology and properties of PE/P-MMTs nanocomposites

WAXD profiles of the resultant nanocomposites are shown in Figure 3. A weak (001) diffraction peak could be observed in the PE/P-MMTs samples. Comparatively, the PE/12MMTs samples showed a strong (001) diffraction peak. TEM images for the microstructures of the resultant products are shown in Figure 4. As expected, only intercalated structure was formed in PE/12MMTs composites even if the content of 12MMTs was very low [Fig. 4(d)]. In contrast, a mixed state of exfoliated and intercalated P-MMTs coexisted in PE matrix [Fig. 4(a–c)]. The content of exfoliated P-MMTs increased gradually with decreasing the P-MMTs content [Fig. 4(e,f)]. This phenomenon was similar to Khalil's work.[30] Actually the MMT contents in the P-PE2 (0.4 wt %) and the P-PE3 (1.0 wt %) are the same as those in the 12PE1 (0.4 wt %) and the 12PE2 (1.0 wt %), respectively. This demonstrates that P-MMTs can be more easily exfoliated and well dispersed in PE matrix, which agrees with other works using polymerizable clay.[16,22–37] Furthermore, the interface between MMTs sheets and PE matrix was so fuzzy that MMTs could not be seen clearly in low-magnification TEM images when the P-MMTs were well exfoliated in PE/P-MMTs nanocomposites (e.g., P-PE2). This results from the strong interaction in the interfacial region. Thus the copolymerization plays an important role in the exfoliation of P-MMTs. The exfoliation degree of PE/P-MMTs and PE/12MMTs can be informed by the gas permeation of the materials when the MMT loading is the same (Table II). Owing to the good dispersion of P-MMTs in PE matrix, P-PE3 and P-PE1 showed better barrier property compared to HOMO and 12PE2. Comparing P-PE3 with P-PE1, it was clearly seen that under the precondition of good dispersion, the higher the content of MMTs was, the better the gas barrier property was. Although 12PE2 (1.0 wt % of MMTs) had a higher content of MMTs than P-PE1 (0.2 wt % of MMTs), oxygen transmission rate of P-PE1 was 43% lower than that of 12PE2. More interestingly, an 80% decrease in oxygen transmission rate of P-PE3 occurred comparing with HOMO sample.

Figure 5 presents EDX patterns and FESEM images of P-PE3 and 12PE3 after extracting with boiling decalin for 48 h. The results showed that the content of carbon element was still high in PE/P-

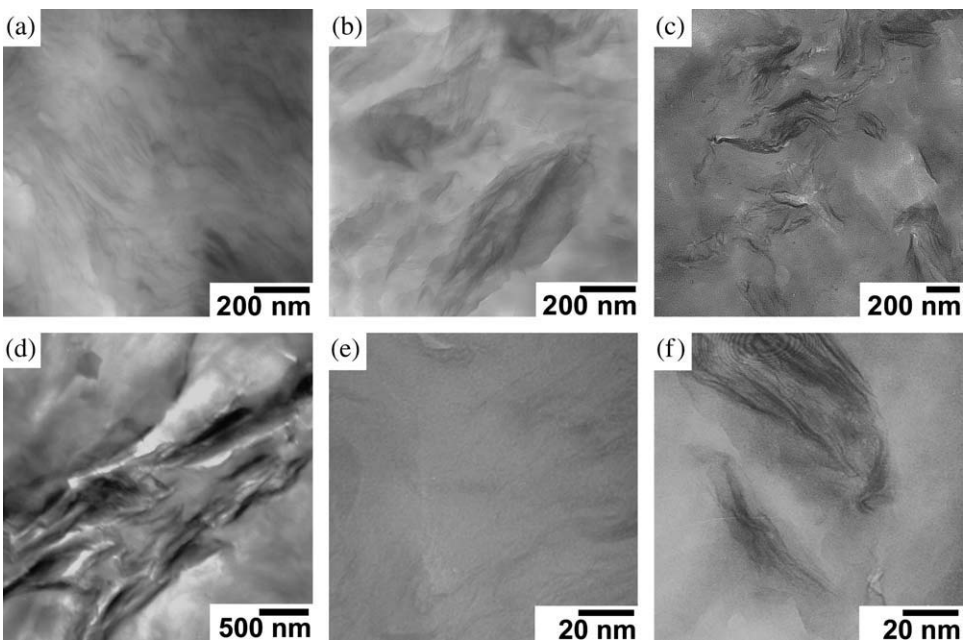

Figure 4 TEM images of (a,e) P-PE2, (b) P-PE3, (c,f) P-PE4, and (d) 12PE1.

TABLE II
The Permeability Coefficient of Oxygen for the Samples at 30°C

Sample	HOMO	P-PE1	P-PE3	12PE2
MMTs content (wt %)	0	0.2	1.0	1.0
Transmission rate (barrer[a])	6.15	1.58	1.20	2.10
P_n/P_h[b]	1	0.257	0.195	0.341

[a] 1 barrer = 10^{-10} cm cm^3 cm^{-2} s cm Hg.
[b] P_n: oxygen transmission rate of the nanocomposite sample; P_h: oxygen transmission rate of the HOMO sample.

MMTs nanocomposites after extraction [Fig. 5(a)], meaning that a large amount of PE remained in the sample, evidenced by the morphology observation [Fig. 5(b,c)]. In contrast, a little amount of carbon element was found in the extracted 12PE3 sample [Fig. 5(d)], and only trace of PE was left [Fig. 5(e,f)]. This extraction experiment confirmed that the strong interaction in the interfacial region between MMTs and PE matrix was formed in PE/P-MMTs nanocomposites compared to PE/12MMTs composites. In the former case, a part of PE chains would be linked to the MMTs surface by electrovalent force after copolymerizing ethylene with P-MMTs. The PE/P-MMTs nanocomposites have been subjected to ^{1}H-NMR and ^{13}C-NMR examinations to determine the occurrence of ethylene copolymerization with the vinyl group on the P-MMTs. Before NMR measurements, the P-PE5 was dipped in concentrated HF solution for a week to remove the MMT sheets and improve the solubility of the remained PE in organic solvent. The residue was filtered, washed with water followed by C_2H_5OH to remove the unreacted polymerizable modifier, and dried before the examination. In Figure 6(a), besides the major chemical shift at $\delta = 1.35$ ppm, which corresponds to C$\boldsymbol{H}_2$ groups in both PE backbone and its branch chain, the spectrum shows a minor chemical shift at $\delta = 3.24$ ppm, which represents the characteristic resonance for the —C$\boldsymbol{H}_2$—NH_3^+ group, and $\delta = 2.05$ ppm, which represents the characteristic resonance for the —C$\boldsymbol{H}_2$—CH_2—NH_3^+ group. The ^{13}C-NMR spectrum [Fig. 6(b)] shows that the produced PE brings methyl branches (marked as *Me*) and long chain branches (longer than six C atoms, marked as Hx^+) that are produced via the insertion of vinyl-terminated PE formed *in situ* through β-hydride elimination or chain transfer to the monomer.[51–54] The chemical shifts and their corresponding characteristic resonances are listed in Figure 6(b). Noticeably the chemical shift $\delta = 43.15$ ppm represents the characteristic resonance for the —CH_2—NH_3^+ group. These results

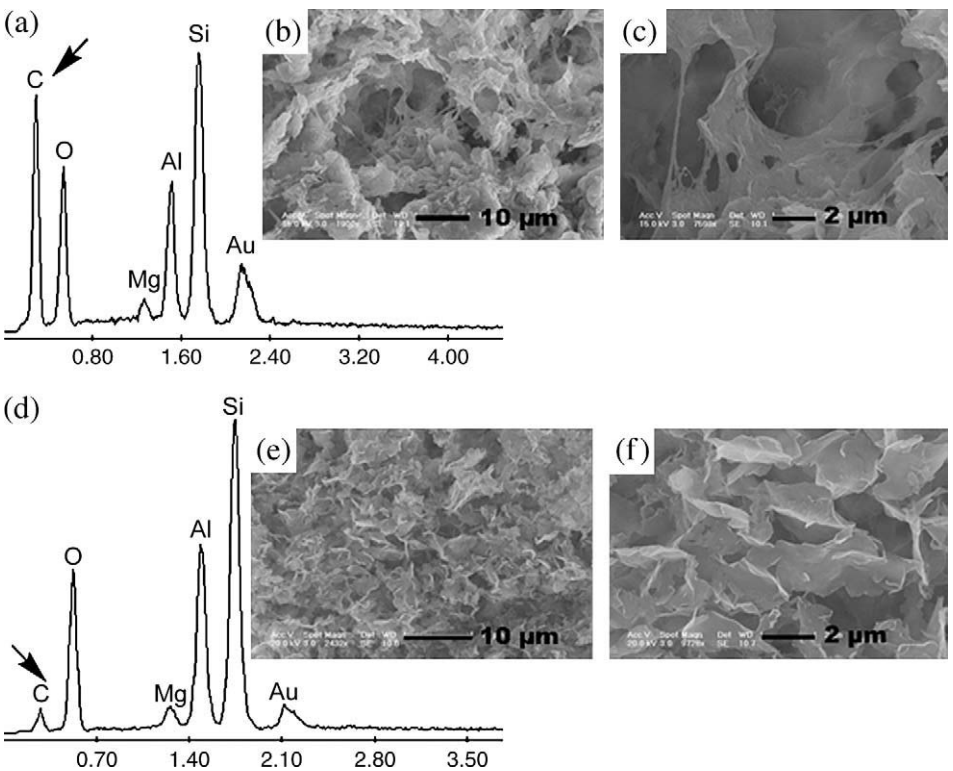

Figure 5 (a) EDX pattern of P-PE3 after extracting pure PE with boiling decalin for 48 h (corresponding to the area shown in the FESEM image (b)); (b) Low-magnification FESEM micrograph of P-PE3 after solvent extraction; (c) High-magnification FESEM micrograph of P-PE3 after solvent extraction; (d) EDX pattern of 12PE3 after extracting PE with boiling decalin for 48 h (corresponding to the area shown in FESEM image (e)); (e) Low-magnification FESEM micrographs of 12PE3 after solvent extraction; (f) High-magnification FESEM micrographs of 12PE3 after solvent extraction.

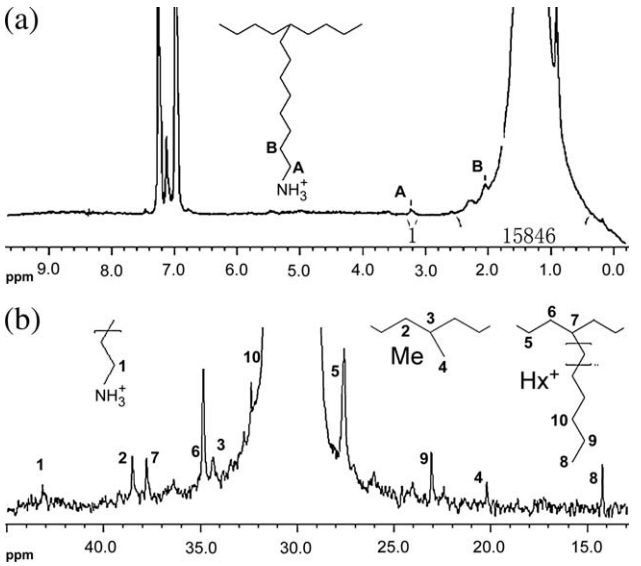

Figure 6 ^{1}H-NMR (a) and 13C-NMR (b) spectra of treated P-PE5 in *o*-DCB-d_4 at 130°C (*Me* stands for methyl branches, Hx^+ stands for long chain branches with more than six C atoms).

confirm that the copolymerization of ethylene with the P-MMTs has been performed successfully. More detailed information about the microstructure of PE/P-MMTs nanocomposites can be obtained by calculation using the ^{1}H-NMR and GPC data.

Taking P-PE5 for example, supposing the integral intensity of $-C\mathbf{H}_2-NH_3^+$ structure is 1, then the integral intensity of other C—H structure is 15,846 [Fig. 6(a)]. Apparently the number of hydrogen atom in $-C_{11}H_{21}-NH_3^+$ structure is much less than that in the backbone C–H structure, so the PE chain can be simplified to be composed of $-CH_2-$. Then the weight percentage of $-C_{11}H_{21}-NH_3^+$ (wt $\%_{-C_{11}H_{21}-NH_3^+}$) structure can be got by formula (1):

$$\text{wt }\%_{-C_{11}H_{21}-NH_3^+} = \frac{I_{-CH_2-NH_3^+} \times \frac{1}{2} \times M_{-C_{11}H_{21}-NH_3^+}}{I_{-CH_2-} \times \frac{1}{2} \times M_{-CH_2-}} \quad (1)$$

Where $I_{-CH_2NH_3^+}$ stands for the integration of $-CH_2-NH_3^+$, I_{-CH_2-} stands for the integration of $-CH_2-$ structure within PE chain. $M_{-C_{11}H_{21}-NH_3^+}$ and M_{-CH_2-} are the molecular weights of $-C_{11}H_{21}-NH_3^+$ and $-CH_2-$. wt $\%_{-CH_{11}H_{21}-NH_3^+}$ turns out to be 0.077%. Furthermore, the reaction efficiency of the polymerizable modifier ($R\%_{PM}$) can be gained:

$$R\%_{PM} = \frac{\text{wt }\%_{-C_{11}H_{21}-NH_3^+}}{\text{wt }\%_{P-MMT} \times \text{wt }\%_{PM}} \quad (2)$$

Here wt $\%_{P\text{-}MMT}$ stands for the content of P-MMTs in the P-PE5, wt $\%_{PM}$ stands for the content of the polymerizable modifier in the P-MMTs sample. $R\%_{PM}$ turns out to be 14.7%. Considering the surface area of MMTs (A_{MMT}) is 700–800 $m^2\ g^{-1}$, the number of polymerizable modifier molecule linked to PE backbone for each MMT sheet ($N_{PM\text{-}M}$) can be calculated:

$$N_{PM-M} = \frac{CEC \times NA \times E\%_{PM} \times R\%_{PM}}{100 \times A_{MMT}/A_{sheet}} \quad (3)$$

Here $E\%_{PM}$ is the cation exchange efficiency, NA is Avogadro constant, A_{sheet} is the surface area of each MMT sheet. Supposing the shape of MMTs is round, then $A_{sheet} = 2\pi\ d^2/4$, and because the aspect of used MMTs is 100–200, hence d (diameter of each sheet) could be 100–200 nm. The average values of A_{MMT} and d have been taken, i.e. 750 m^2/g and 150 nm, respectively. Thus $N_{PM\text{-}M}$ should be 4014. Combining with the GPC data, the number of polymerizable modifier molecule linked to each PE molecule ($N_{PM\text{-}P}$) can also be got:

$$N_{PM-P} = \frac{\text{wt }\%_{-C_{11}H_{21}-NH_3^+}/M_{-C_{11}H_{21}-NH_3^+}}{PDI_{EX} \times (\text{wt }\%_{EX} - \text{wt }\%_{P-MMT})/M_{wEX}} \quad (4)$$

Where wt $\%_{EX}$ is the weight percentage of extracted P-PE5 divided by sample weight before extraction. M_{nEX}, M_{wEX}, and PDI_{EX} (polydispersity index) are M_n, M_w, and PDI data of the extracted P-PE5 after HF treatment. $N_{PM\text{-}P}$ turns out to be 1.2. This proved that it had a crosslinking structure composed of MMTs and polymer chains. Further, the value of $N_{PM\text{-}M}/N_{PM\text{-}P}$ stands for the number of PE chains linked to each MMT sheet, and it turns out to be 3345. These results only fit for the case of P-PE5. It is well known that naturally occurring layered silicates (such as MMTs) are inhomogenous across layers,[55] thus such calculation serves only as an approximate guide to the microstructure of PE/P-MMTs nanocomposites.

As expected, the formation of special microstructure in PE/P-MMTs nanocomposites led to a significant improvement in mechanical properties at relatively low MMT content. The nanocomposites (P-PE1 and P-PE3) showed a better performance than pure PE (HOMO) in tensile modulus, tensile strength, and especially elongation at break (c.a. 2000%). The deformation behavior of PE/P-MMTs nanocomposites has been reported in another work by us;[56] it was found that the synchronous improvements in stress and toughness were attributed to the synergistic movement of PE matrix and P-MMTs.

Formation mechanism of the morphology of PE/P-MMTs nanocomposites during *in situ* polymerization

The earlier results showed that the dispersion state of P-MMTs in PE matrix depended on the

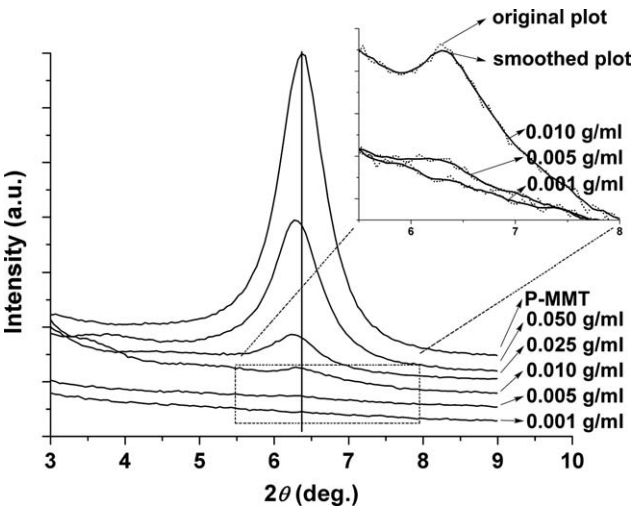

Figure 7 WAXD profiles of P-MMTs and swollen P-MMTs at different concentration in toluene (0.001–0.050 g/mL).

concentration of P-MMTs. Generally OMMTs are well known in their ability for swelling and gel formation in organic media, and the concentration of OMMTs influences their aggregation states.[15,17–20] The dispersion states of OMMTs in organic solvent are multiscale organization of nanoclays, i.e., swelling at the macroscopic scale to form gels, and interplatelets swelling at nanoscopic scale.[19–21] In our case, the interlayers of P-MMTs swell slightly in toluene according to WAXD results [Fig. 7]. The number of platelets (n) in tactoids can be calculated according to the reference method[15] using Scherrer law:

$$L = \frac{k\lambda_{Cu}}{\beta_{1/2}\cos\theta} \Rightarrow n = \frac{L}{d_{001} + 1nm} \quad (5)$$

Here L stands for the size of the diffractant objects, λ_{Cu} is the wavelength of the copper emission, and θ is the Bragg angle, k is a corrective factor (here $k = 0.9$), $\beta_{1/2}$ is the peak width at half-height. It could be got that $n = 3$ in the concentration of 0.050, 0.025, 0.010, and 0.005 g/mL. The plot of 0.001 g/mL shows no signal because of the low concentration of P-MMTs. But based on the results, we had already got, it can be inferred that the number of platelets (n) in tactoids of P-MMTs at very low concentration is probably 3. The results showed a good agreement with Burgentzlé's work.[15] FESEM images show that swollen P-MMTs have formed globose gels in toluene at micrometer scale [Fig. 8(a,b)]. The swollen P-MMTs suspensions were dripped onto silicon wafer to observe the aggregation states of P-MMTs in toluene. The data in Figure 9 are an average value of the diameters taken from at least 50 aggregates, based on the diameters of the aggregates in the FESEM images. An example of the detailed diameter distribution is given in Figure 9(a). The diameters of the aggregates increased with the concentration of P-MMTs in the suspension in the concentration ranging from 0.0001 to 0.0016 g/mL [Fig. 9(b)], which is also the concentration range of the dispersed P-MMTs for the filling polymerization in this work. On the above results, a schematic diagram for the evolution process of the microstructure in PE/P-MMTs nanocomposites is shown in Figure 10. This can explain why the aggregation states of P-MMTs in polymerization media influence the microstructure of the resultant nanocomposites during the filling polymerization. Metallocene catalyst should be uniformly dispersed in the reaction system due to its good solubility in toluene. At the beginning of polymerization, some of the modifiers on the outer side of the swollen P-MMT aggregates are linked to the PE chains through copolymerization. Under the mechanical stir, compared to PE/12MMTs system during polymerization, a stronger shear force acting on the surface of MMT sheets will be formed due to the existence of the PE chains (no matter the chains are dissolving in the solvent or folding to form crystallites) connected to the P-MMTs. This can be justified by examining the influence of the mechanical stirring rate on the dispersion states of P-MMTs.

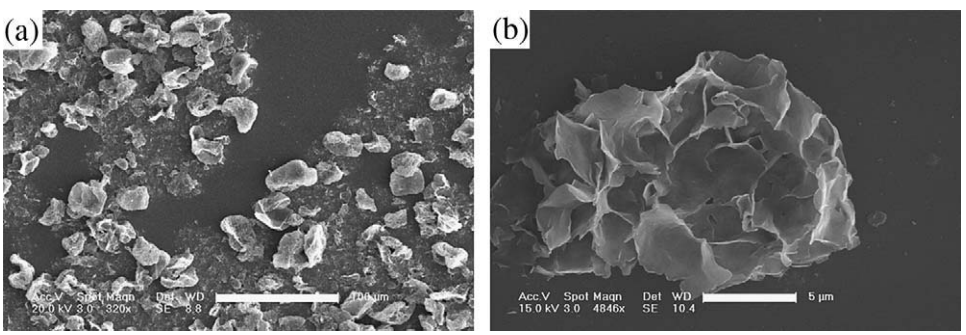

Figure 8 Low-magnification (a) and high-magnification (b) FESEM micrographs of swollen P-MMT aggregates at concentration 0.0006 g/mL.

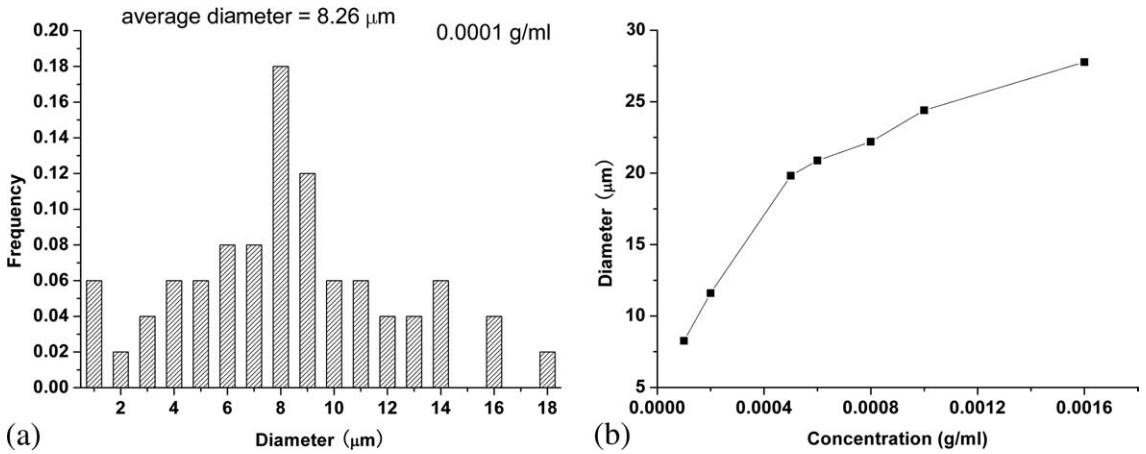

Figure 9 Diameter distribution of swollen P-MMTs aggregates at different concentration (0.0001–0.0016 g/mL).

Figure 11 presents the influence of the mechanical stirring rate on the dispersion states of P-MMTs. Here the concentration of P-MMTs in the reaction system was 0.0008 g/mL. The polymerization time was about 50 min for each sample, and the content of the P-MMTs in PE/P-MMTs nanocomposites was 3.0 wt %. According to the results that will be discussed later, when the polymerization time was above 45 min, prolonging time did not obviously affect the exfoliation of the P-MMTs. Thus the difference in the microstructures of the resultant samples could reflect the influence of mechanical stirring rate. Here K is defined to be an index of the degree of exfoliation:

$$K = \frac{I_{\mathrm{P-MMT}}}{\mathrm{wt}\ \%_{\mathrm{P-MMT}}} \Big/ \frac{I_{\mathrm{PE}}}{\mathrm{wt}\ \%_{\mathrm{PE}}} \tag{6}$$

$I_{\mathrm{P\text{-}MMT}}$ and I_{PE} stand for the integral of the intensities of (001) diffraction peak of P-MMT and the peak of PE located at $2\theta = 15\text{–}25^{\circ}$ on the WAXD profiles, respectively; wt $\%_{\mathrm{P\text{-}MMT}}$ and wt $\%_{\mathrm{PE}}$ represent the weight percentages of P-MMTs and PE in the nanocomposites, respectively. As the integral of the intensity of X-ray diffraction peak is in proportion to the amount of the corresponding structure, K can reflect the degree of exfoliation of the P-MMTs. Here the PE crystallite is used as internal standard. Only the unexfoliated P-MMTs would contribute to the intensity of the diffraction peak of P-MMT. The influence of the P-MMTs content is eliminated by dividing $I_{\mathrm{P\text{-}MMT}}$ by wt $\%_{\mathrm{P\text{-}MMT}}$; and the influence of crystallinity of the PE is eliminated by dividing I_{PE} by wt $\%_{\mathrm{PE}}$. So the small K means that the more P-MMTs are exfoliated. The results showed that the larger the stirring rate was, the smaller K was [Fig. 11(b)]. This implies that more P-MMTs platelets in the nanocomposites prepared at 350 rpm and 600 rpm were exfoliated comparing with the one prepared at 110 rpm. Inset TEM images in Figure 11(a) confirmed the earlier results. Under a high stirring rate, owing to the presence of PE chains linked to the surface of P-MMTs, the shear force will be

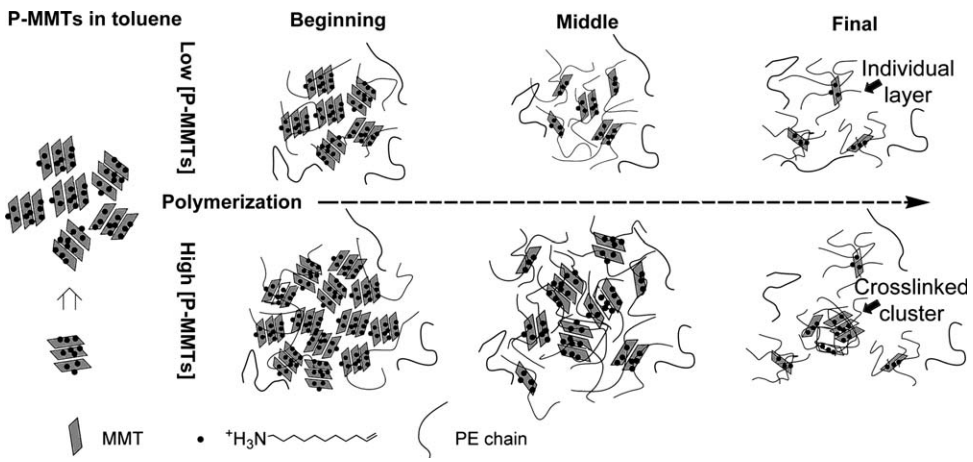

Figure 10 Schematic illustrations of the formation process of PE/P-MMTs nanocomposites during *in situ* ethylene polymerization in the presence of P-MMTs with different concentration.

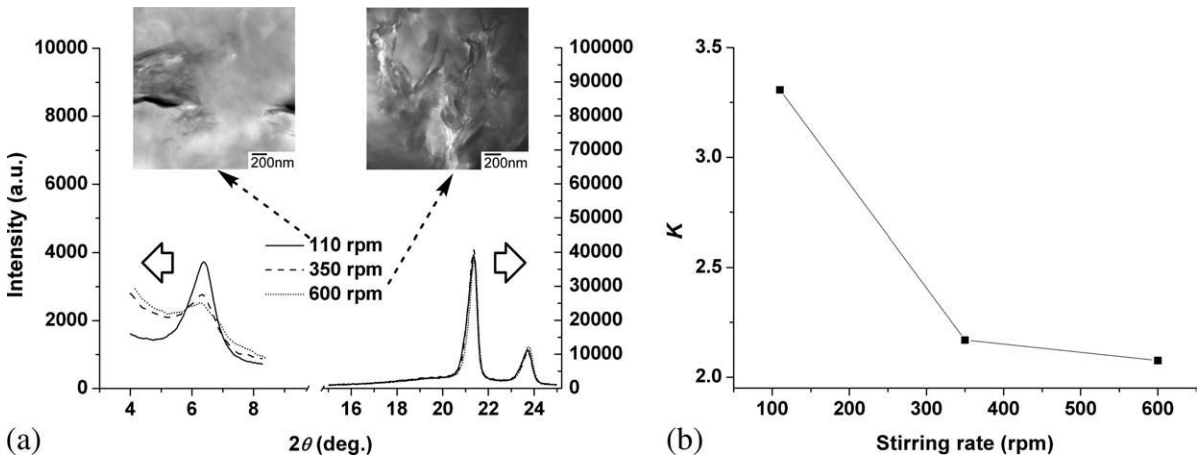

Figure 11 (a) WAXD profiles of PE/P-MMTs composites (P-MMTs ≈ 3.0 wt %) prepared at stirring rate 110, 350, 600 rpm and their corresponding TEM images; (b) Relationship of *K* value with stirring rate, *K* value is an index of the exfoliation degree of MMTs.

efficiently transmitted to P-MMT platelets to aid their exfoliation. Thus adjusting the mechanical stirring rate would lead to the formation of the nanocomposites with different microstructures when keeping other polymerization conditions the same. However, as shear force could not increase illimitably when the stirring rate went up, there was little difference in the degree of exfoliation of the nanocomposites prepared at 350 and 600 rpm, meaning that the microstructure difference in these nanocomposites was small. The conclusion that the driving force for the exfoliation of P-MMTs is the shear force transmitted through the polymerizable agent helps to explain the phenomenon that the P-MMTs containing modifiers with long chains are more exfoliated than those with short chains.[16,24,37] The polymerizable modifiers of P-MMTs with long chains are easier to be involved in the copolymerization and achieve stronger shear force than the polymerizable modifiers with short chains.

As shown in Figure 10, the outer P-MMT sheets tend to be peeled away under the shear force, but those in the inner of the swollen P-MMT aggregates have a tendency to crosslink as the outer P-MMTs platelets block their way to be exfoliated. As the polymerization continues, the inner P-MMT sheets will be exposed after the outer P-MMT sheets are peeled away. At the same time, the crosslinking process in the inner of the swollen P-MMT aggregates is also going on due to the presence of a lot of P-MMT sheets, thus the crosslinking process is competitive with the exfoliation process. As a result, the dispersion state of P-MMTs in PE matrix strongly depends on the size of its aggregates. When the diameters of the aggregates are large, more P-MMT sheets are easy to be crosslinked; otherwise, P-MMT sheets are easy to be exfoliated. Thus the percentage of exfoliated MMT sheets in PE/P-MMTs nanocomposites increases with decreasing the concentration of P-MMTs in the reaction systems. TEM image of P-PE4

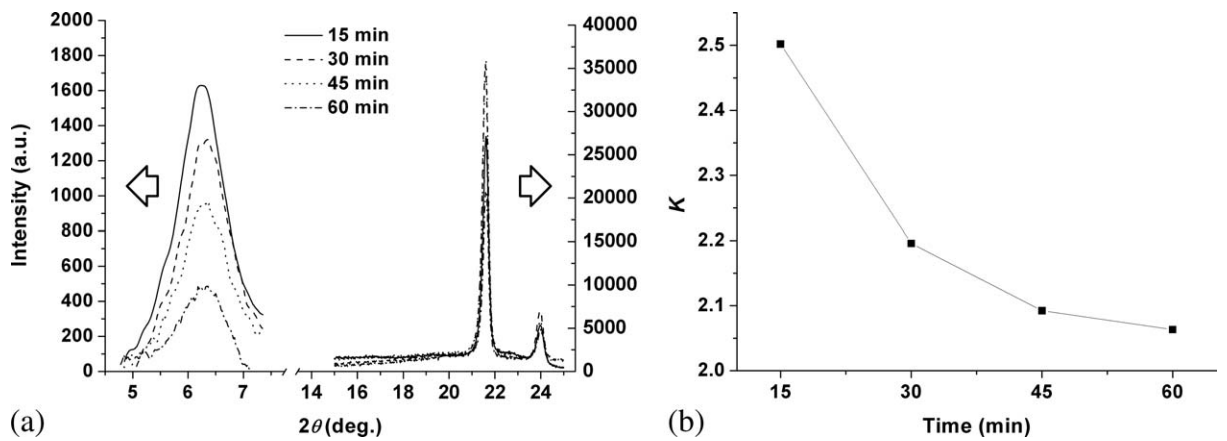

Figure 12 (a) WAXD profiles of PE/P-MMTs samples prepared at different polymerization time; (b) Relationship of *K* value with polymerization time, *K* value is an index of the exfoliation degree of MMTs.

sample provides a proof of this explanation [Fig. 4(f)]. There are individual MMT sheets near the cluster edge of the intercalated P-MMTs.

The dependence of WAXD profiles of PE/P-MMTs nanocomposites on polymerization time supported the earlier discussion about the dispersion process of the P-MMTs. Here the concentration of P-MMTs is 0.0010 g/mL. The samples were obtained at different polymerization time (15, 30, 45, and 60 min), and their corresponding P-MMT contents were 3.7, 3.1, 2.2, and 1.6 wt %, respectively, according to the results of TGA. The (001) diffraction peak on the WAXD profiles do not shift with polymerization time [Fig. 12(a)], implying that the metallocene catalyst almost did not intercalate the interlayer of P-MMTs during the filling polymerization, but probably diffused into the inside of P-MMTs aggregates, where the crosslinking of P-MMTs will take place. Otherwise, there will be not the dependence of the microstructures of the resultant PE/P-MMTs nanocomposites on the concentration of P-MMTs in reaction system. The data were processed in the same way as the investigation of the influence of stirring rate. It could be seen that the proportion of the exfoliated structure increased with the polymerization time [Fig. 12(b)]. Comparatively, the change of K value became small when the polymerization time prolonged above 45 min, suggesting that the exfoliation would slow down and even stop when the crosslinked structure was formed and finally completed. The above results confirm that the exfoliation of P-MMTs aggregates is realized from exterior to interior.

CONCLUSIONS

By a filling polymerization method, the P-MMTs originated from undec-10-enylammonium chloride (a polymerizable modifier) were chemically linked to the backbones of some of PE chains during ethylene polymerization. As a result, the interfacial interaction between PE and MMT was strengthened, and the dispersion of P-MMTs was better than nonpolymerizable organophilic MMTs. During the filling polymerization, the shear force formed by mechanical stirring, which would be efficiently transferred to the MMT platelets via the interaction between polymer chains linked to the surface of MMT sheets and the solvents molecules, is the driving force for the exfoliation of MMT sheets during the filling polymerization. Owing to the presence of the polymerizable modifier incorporated in the polymer backbone, this driving force made polymerizable organophilic clay more easily exfoliated than nonpolymerizable organophilic clay during preparing PE/MMT nanocomposites via filling polymerization. In this case, the P-MMT sheets were gradually peeled away from the aggregates of swollen P-MMTs in toluene. Because of the strong dependence of the size of the organoclay aggregates on its concentration in the organic medium, the dispersion states of P-MMTs in the PE/P-MMTs nanocomposites strongly depended on the concentration of P-MMTs in the reaction systems. The exfoliated dispersion of the P-MMTs would easily occur in the presence of relatively low content of P-MMTs. We believe that a similar process for the microstructure formation occurs in other polymer/clay nanocomposites via filling polymerization. It should be noticed that preventing the formation of large P-MMT aggregates in the reaction system during the filling polymerization will promote exfoliated dispersion of P-MMT sheets in the polymer nanocomposites.

References

1. Okada, A.; Kawasumi, M.; Kurauchi, T.; Kamigaito, O. Polym Prepr (Am Chem Soc Div Polym Chem) 1987, 28, 447.
2. Okada, A.; Kawasumi, M.; Kurauchi, T.; Kamigaito, O. U.S. Pat. 4,739,007 (1988).
3. Okada, A.; Fukushima, A.; Kawasumi, M.; Inagaki, S.; Usuki, A.; Sugiyama, S.; Kurauchi, T. Chem Abstr 1987, 107, 60084.
4. Alexandre, M.; Dubois, P. Mater Sci Eng 2000, 28, 1.
5. Vaia, R. A.; Giannelis, E. P. Macromolecules 1997, 30, 7990.
6. Decker, C.; Keller, L.; Zahouily, K.; Benfarhi, S. Polymer 2005, 46, 6640.
7. Horsch, S.; Serhatkulu, G.; Gulari, E.; Kannan, R. M. Polymer 2006, 47, 7485.
8. Hasegawa, N.; Okamoto, H.; Kato, M.; Usuki, A.; Sato, N. Polymer 2003, 44, 2933.
9. Tabtiang, A.; Lumlong, S.; Venables, R. A. Polym Plast Technol Eng 2000, 39, 293.
10. Huang, X. Y.; Brittain, W. J. Macromolecules 2001, 34, 3255.
11. Xie, W.; Gao, Z. M.; Pan, W. P.; Hunter, D.; Singh, A.; Vaia, R. Chem Mater 2001, 13, 2979.
12. Bhiwankar, N. N.; Weiss, R. A. Polymer 2006, 47, 6684.
13. Weimer, M. W.; Chen, H.; Giannelis, E. P.; Sogah, D. Y. J Am Chem Soc 1999, 121, 1615.
14. Di, J.; Sogah, D. Y. Macromolecules 2006, 39, 5052.
15. Burgentzlé, D.; Duchet, J.; Gérard, J. F.; Jupin, A.; Fillon, B. J Colloid Interface Sci 2004, 278, 26.
16. Owusu-Adom, K.; Guymon, C. A. Macromolecules 2009, 42, 180.
17. Lagaly, G.; Malberg, R. Colloids Surf 1990, 49, 11.
18. Farmer, B. L.; Vaia, R. A.; Bharadwaj, R. K. Polym Prepr 2001, 42, 21.
19. Moraru, V. N. Appl Clay Sci 2001, 19, 11.
20. Jordan, J. W. J Phys Colloid Chem 1949, 53, 294.
21. Zhong, Y.; Wang, S. Q. J Rheol 2003, 47, 483.
22. Zeng, C.; Lee, L. J. Macromolecules 2001, 34, 4098.
23. Tseng, C. R.; Wu, J. Y.; Lee, H. Y.; Chang, F. C. J Appl Polym Sci 2002, 85, 1370.
24. Bottino, F. A.; Fabbri, E.; Fragalà, I. L.; Malandrino, G.; Orestano, A.; Pilati, F.; Pollicino, A. Macromol Rapid Commun 2003, 24, 1079.
25. Fu, X.; Qutubuddin, S. Polymer 2001, 42, 807.
26. Qutubuddin, S.; Fu, X. A.; Tajuddin, Y. Polym Bull 2002, 48, 143.
27. Wang, H. W.; Chang, K. C.; Yeh, J. M.; Liou, S. J. J Appl Polym Sci 2004, 91, 1368.
28. Zhong, Y.; Zhu, Z. Y.; Wang, S. Q. Polymer 2005, 46, 3006.

29. Samakande, A.; Hartmann, P. C.; Cloete, V.; Sanderson, R. D. Polymer 2007, 48, 1490.
30. Khalil, H.; Mahajan, D.; Rafailovich, M. Polym Int 2005, 54, 428.
31. Zang, Y. L.; Xu, W. J.; Liu, G. P.; Qiu, D. Y.; Su, S. P. J Appl Polym Sci 2009, 111, 813.
32. Tan, H. L.; Nie, J. Macromol React Eng 2007, 1, 384.
33. Zhang, Y. H.; Cai, Q. Y.; Jiang, Z. J.; Gong, K. C. J Appl Polym Sci 2004, 92, 2038.
34. Owusu-Adom, K.; Schall, J.; Guymon, A. Macromolecules 2009, 42, 3275.
35. Diaconu, G.; Mičušík, M.; Bonnefond, A.; Paulis, M.; Leiza, J. R. Macromolecules 2009, 42, 3316.
36. Shin, S. Y. A.; Simon, L. C.; Soares, J. B. P.; Scholz, G. Polymer 2003, 44, 5317.
37. Fu, X. A.; Qutubuddin, S. Polym Eng Sci 2004, 44, 345.
38. Alexandre, M.; Martin, E.; Dubois, P.; Garcia-Marti, M. Macromol Rapid Commun 2000, 21, 931.
39. He, A. H.; Hu, H. Q.; Huang, Y. J.; Dong, J. Y.; Han, C. C. Macromol Rapid Commun 2004, 25, 2008.
40. Sun, T.; Garces, J. M. Adv Mater 2002, 14, 128.
41. Bergman, J. S.; Chen, H.; Giannelis, E. P.; Thomas, M. G.; Coates, G. W. Chem Commun 1999, 21, 2179.
42. Lee, D. H.; Kim, H. S.; Yoon, K. B.; Min, K. E.; Seo, K. H.; Noh, S. K. Sci Technol Adv Mater 2005, 6, 457.
43. Wei, L. M.; Tang, T.; Huang, B. T. J Polym Sci Part A: Polym Chem 2004, 42, 941.
44. Liu, C. B.; Tang, T.; Wang, D.; Huang, B. T. J Polym Sci Part A: Polym Chem 2003, 41, 2187.
45. Ray, S.; Galgali, G.; Lele, A.; Sivaram, S. J Polym Sci Part A: Polym Chem 2005, 43, 304.
46. Gagne, M. R.; Stern, C. L.; Marks, T. J. J Am Chem Soc 1992, 114, 275.
47. Balazs, A. C.; Singh, C.; Zhulina, E. Macromolecules 1998, 31, 8370.
48. Kuznetsov, D. V.; Balazs, A. C. J Chem Phys 2000, 113, 2479.
49. Grieken, R.; Martín, C.; Moreno, J.; Prieto, O.; Bravo, J. M. Macromol Symp 2007, 259, 174.
50. Hammawa, H.; Wanke, S. E. Polym Int 2006, 55, 426.
51. Lai, S. Y.; Wilson, J. R.; Knight, G. W.; Stevens, J. C. (to Dow Chemical Corporation). U.S. Pat. 5,272,236 (1993).
52. Wang, W. J.; Yan, D.; Zhu, S.; Hamielec, A. E. Macromolecules 1998, 31, 8677.
53. Kolodka, E.; Wang, W. J.; Zhu, S.; Hamielec, A. E. J Appl Polym Sci 2004, 92, 307.
54. Stapleton, R. A.; Chai, J.; Nuanthanom, A.; Flisak, Z.; Nele, M.; Ziegler, T.; Rinaldi, P. L.; Soares, J. B. P.; Collins, S. Macromolecules 2007, 40, 2993.
55. Krishnamoorti, R.; Giannelis, E. P. Macromolecules 1997, 30, 4097.
56. Ren, C. Y.; Jiang, Z. Y.; Du, X. H.; Men, Y. F.; Tang, T. J Phys Chem B 2009, 113, 14118.